Supporting Information

New-type $K_{0.7}Fe_{0.5}Mn_{0.5}O_2$ Cathode with an Expanded and Stabilized Interlayer Structure for High-Capacity Sodium-Ion Batteries

Xuanpeng Wang [a], Ping Hu [a], Chaojiang Niu *, [a], Jiashen Meng[a], Xiaoming Xu [a], Xiujuan Wei [a], Chunjuan Tang [a, b], Wen Luo [a], Liang Zhou [a], Qinyou An [a] and Liqiang Mai *, [a]

X. P. Wang, P. Hu, Dr. C. J. Niu, J. S. Meng, X. M. Xu, X. J. Wei, W. Luo, Prof. L. Zhou, Dr. Q. Y. An, Prof. L. Q. Mai, State Key Laboratory of Advanced Technology for Materials Synthesis and Processing, Wuhan University of Technology, Wuhan 430070, China

Dr. C. J. Tang, Department of Mathematics and Physics, Luoyang Institute of Science and Technology, Luoyang 471023, PR China

E-mail: mlq518@whut.edu.cn; niuchaojiang11@whut.edu.cn

Keywords: New-type, cathode materials, enlarged and stabilized interlayer structure, high capacity, sodium-ion batteries

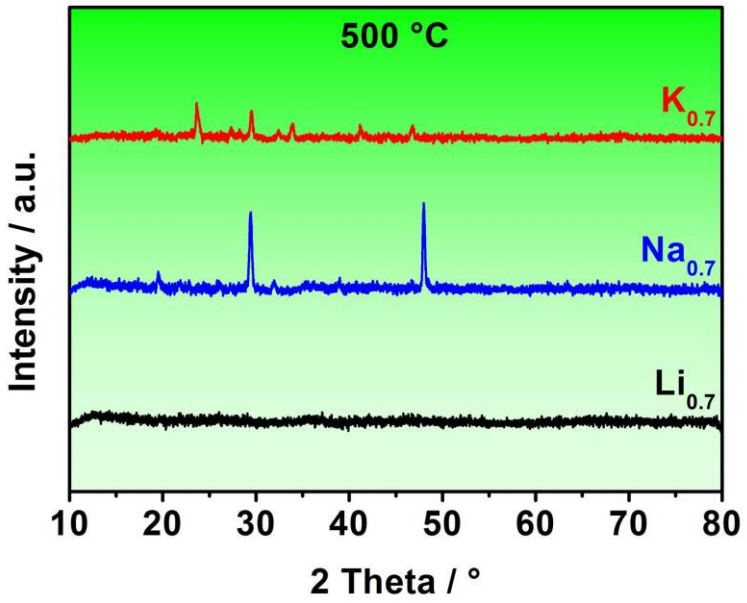

Figure S1. XRD patterns of the $K_{0.7}Fe_{0.5}Mn_{0.5}O_2$, $Na_{0.7}Fe_{0.5}Mn_{0.5}O_2$ and $Li_{0.7}Fe_{0.5}Mn_{0.5}O_2$ were pre-sintered at 500 ℃ for 2 h in air.

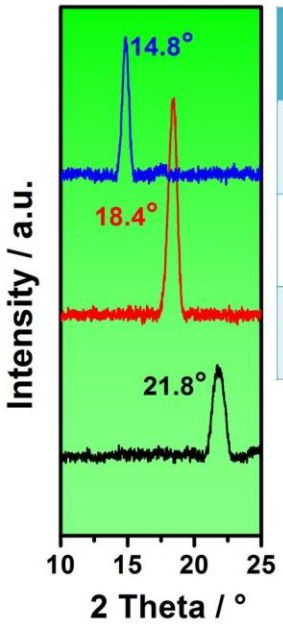

	$Li_{0.7}$	$Na_{0.7}$	$K_{0.7}$
2 $Theta_{(002)}$ / °	21.8	18.4	14.8
D-spacing / Å	4.73	5.58	6.94
R_{M^+} (M=Li, Na, K) / Å	1.33	0.98	0.69

Bragg Equation: $D=\frac{n\lambda}{2\sin\theta}$

Figure S2. The degree values and corresponded d-spacing of the (002) plane for $K_{0.7}Fe_{0.5}Mn_{0.5}O_2$, $Na_{0.7}Fe_{0.5}Mn_{0.5}O_2$ and $Li_{0.7}Fe_{0.5}Mn_{0.5}O_2$.

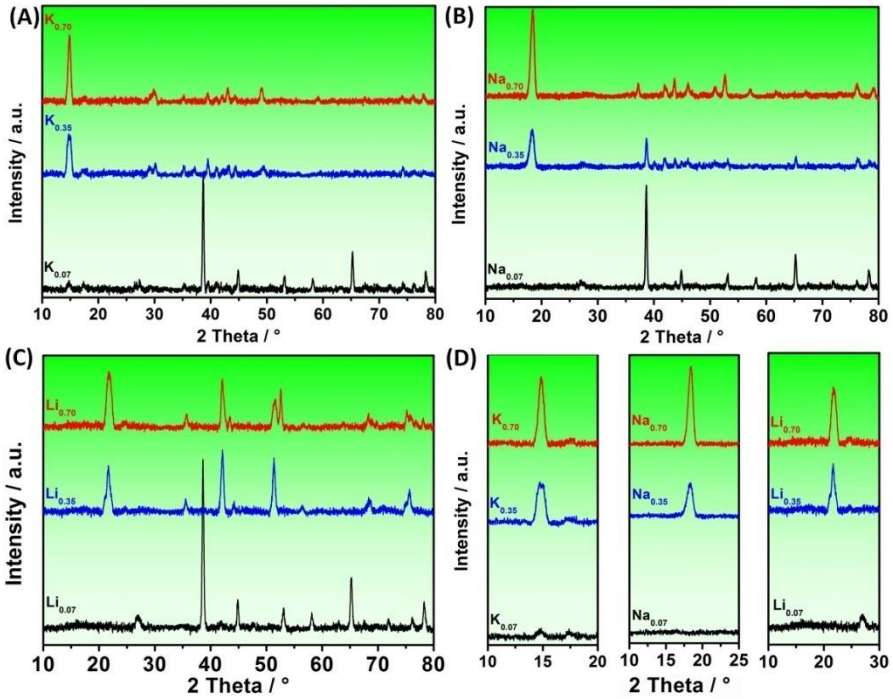

Figure S3. XRD patterns of the $K_xFe_{0.5}Mn_{0.5}O_2$ (A), $Na_xFe_{0.5}Mn_{0.5}O_2$ (B) and $Li_xFe_{0.5}Mn_{0.5}O_2$ (C) ($0.07 \leq x \leq 0.7$). The (002) diffraction peaks details of three samples (D).

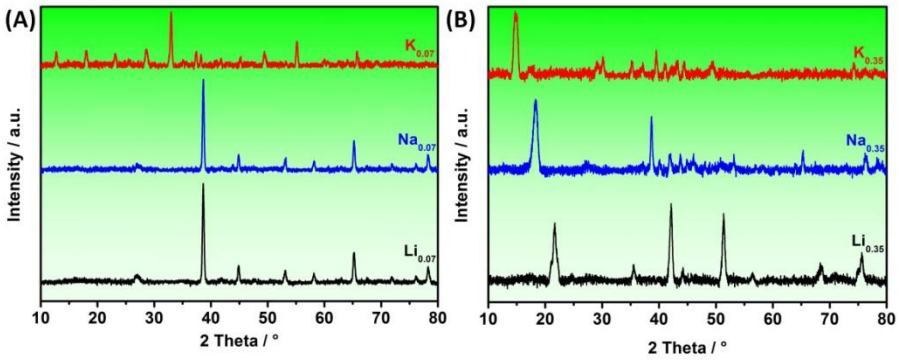

Figure S4. (A) XRD patterns of the $K_{0.07}Fe_{0.5}Mn_{0.5}O_2$, $Na_{0.07}Fe_{0.5}Mn_{0.5}O_2$ and $Li_{0.07}Fe_{0.5}Mn_{0.5}O_2$. (B) XRD patterns of the $K_{0.35}Fe_{0.5}Mn_{0.5}O_2$, $Na_{0.35}Fe_{0.5}Mn_{0.5}O_2$ and $Li_{0.35}Fe_{0.5}Mn_{0.5}O_2$.

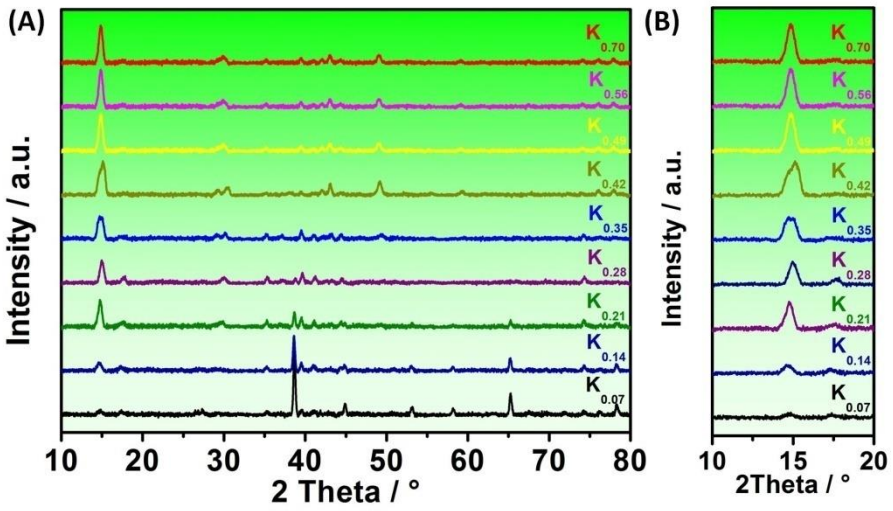

Figure S5. XRD patterns (A) and the (002) diffraction peaks details (B) of the $K_xFe_{0.5}Mn_{0.5}O_2$ ($0.07 \leq x \leq 0.7$).

Table S1. The ICP test results of the $K_{0.7}Fe_{0.5}Mn_{0.5}O_2$, $Na_{0.7}Fe_{0.5}Mn_{0.5}O_2$ and $Li_{0.7}Fe_{0.5}Mn_{0.5}O_2$ after washing with deionized water.

	Mass concentration		Ratios
$Li_{0.7}Fe_{0.5}Mn_{0.5}O_2$	Li	18.41%	Li: Fe: Mn = 0.700:0.503:0.519
	Fe	18.90%	
	Mn	19.20%	
$Na_{0.7}Fe_{0.5}Mn_{0.5}O_2$	Na	17.62%	Na: Fe: Mn = 0.700:0.496:0.518
	Fe	17.84%	
	Mn	18.32%	
$K_{0.7}Fe_{0.5}Mn_{0.5}O_2$	K	24.32%	K: Fe: Mn = 0.700:0.502:0.523
	Fe	18.68%	
	Mn	24.91%	

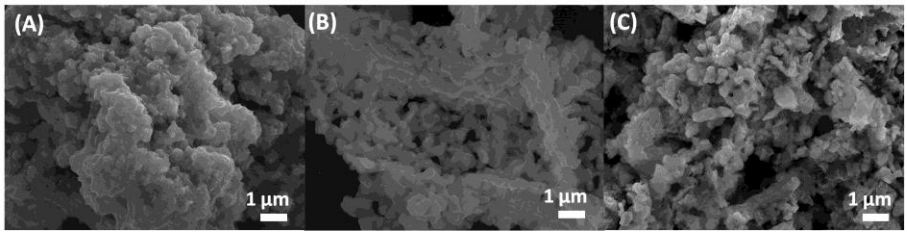

Figure S6. SEM images of $K_{0.7}Fe_{0.5}Mn_{0.5}O_2$, sintered at 600 (A), 800 (B) and 1000 ℃ (C), respectively.

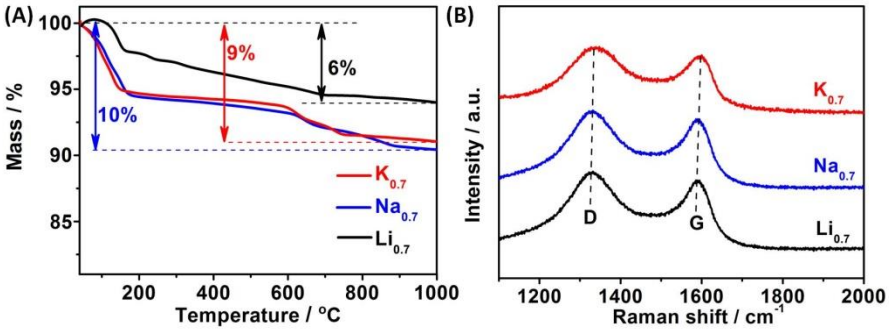

Figure S7. TGA curves (A) and Raman spectra (B) of $K_{0.7}Fe_{0.5}Mn_{0.5}O_2$, $Na_{0.7}Fe_{0.5}Mn_{0.5}O_2$ and $Li_{0.7}Fe_{0.5}Mn_{0.5}O_2$, respectively.

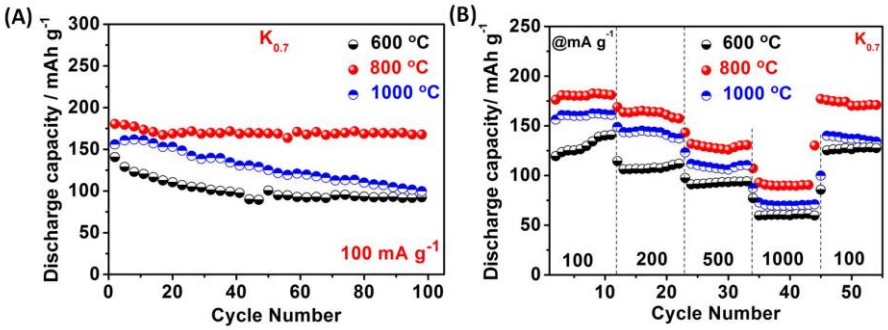

Figure S8. Cycling performance (A) and rates performance (B) of $K_{0.7}Fe_{0.5}Mn_{0.5}O_2$, sintered at 600, 800 and 1000 ℃, respectively.

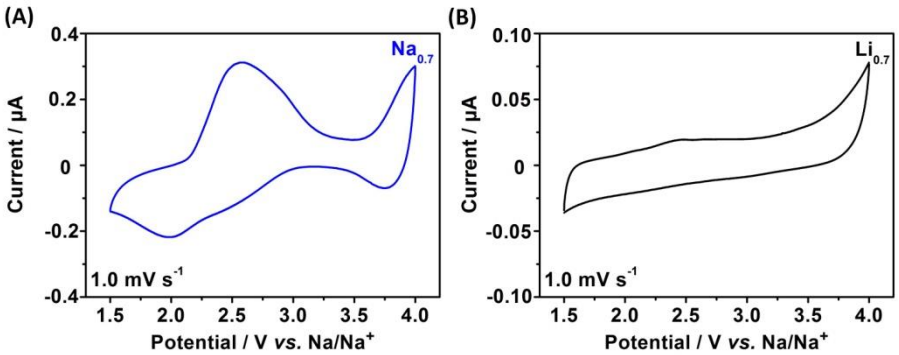

Figure S9. Cyclic voltammograms of $Na_{0.7}Fe_{0.5}Mn_{0.5}O_2$ (A) and $Li_{0.7}Fe_{0.5}Mn_{0.5}O_2$ (B) at a scan rate of 1.0 mV s^{-1} in the electrochemical window of 1.5 to 4.0 V *vs.* Na/Na^+.

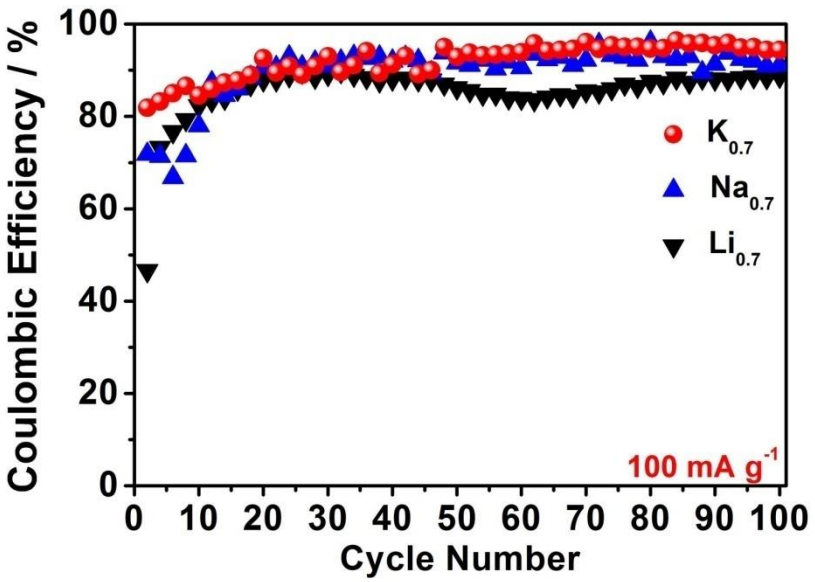

Figure S10. Columbic efficiency of the $K_{0.7}Fe_{0.5}Mn_{0.5}O_2$, $Na_{0.7}Fe_{0.5}Mn_{0.5}O_2$ and $Li_{0.7}Fe_{0.5}Mn_{0.5}O_2$, at current density of 100 mA g^{-1}.

Table S2. The *ex-situ* ICP test results of $K_{0.7}Fe_{0.5}Mn_{0.5}O_2$ at different electrochemical states.

	K: Na: Fe
Before cycle	0.700 : 0.417 : 0.499
Charge to 4.0 V	0.101 : 0.004 : 0.497
Discharge to 1.5 V	0.107 : 0.982 : 0.500
After 2 cycles	0.105 : 0.976 : 0.498
After 10 cycles	0.106 : 0.975 : 0.496
After 50 cycles	0.101 :0.982 : 0.495
After 100 cycles	0.101 : 0.980 : 0.493

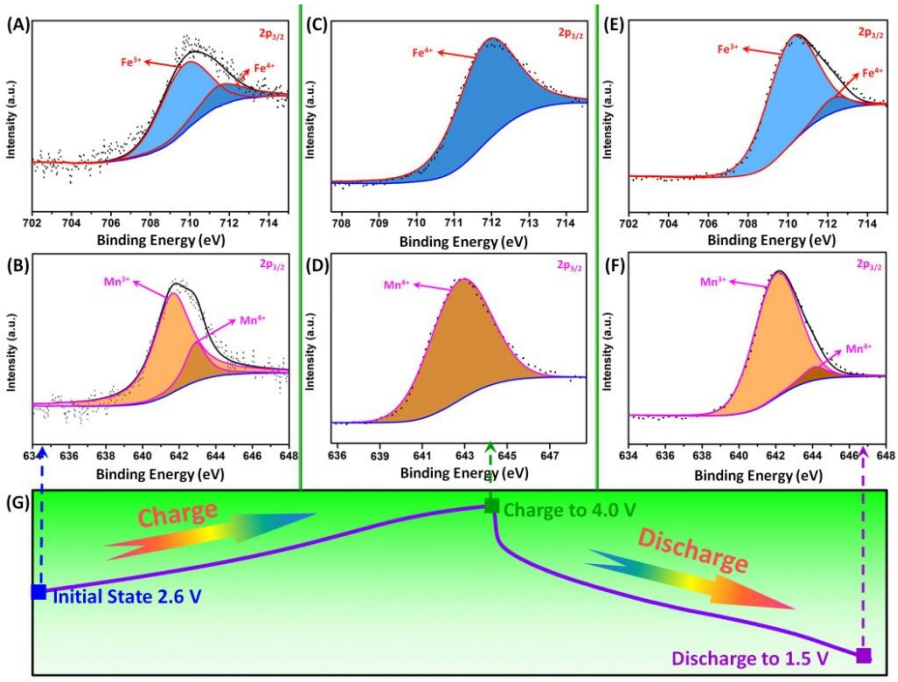

Figure S11. X-ray photoelectron spectra (XPS) for $K_{0.7}Fe_{0.7}Mn_{0.3}O_2$ surface, curve fitting for $Fe2p_{3/2}$ (A) and $Mn2p_{3/2}$ (B) at initial state 2.6 V. XPS for $K_{0.7}Fe_{0.7}Mn_{0.3}O_2$ surface, curve fitting for $Fe2p_{3/2}$ (C) and $Mn2p_{3/2}$ (D) when charged to 4.0 V. XPS for $K_{0.7}Fe_{0.7}Mn_{0.3}O_2$ surface, curve fitting for $Fe2p_{3/2}$ (E) and $Mn2p_{3/2}$ (F) when discharged to 1.5 V. (G) Evolution of cell voltage of $K_{0.7}Fe_{0.7}Mn_{0.3}O_2$.

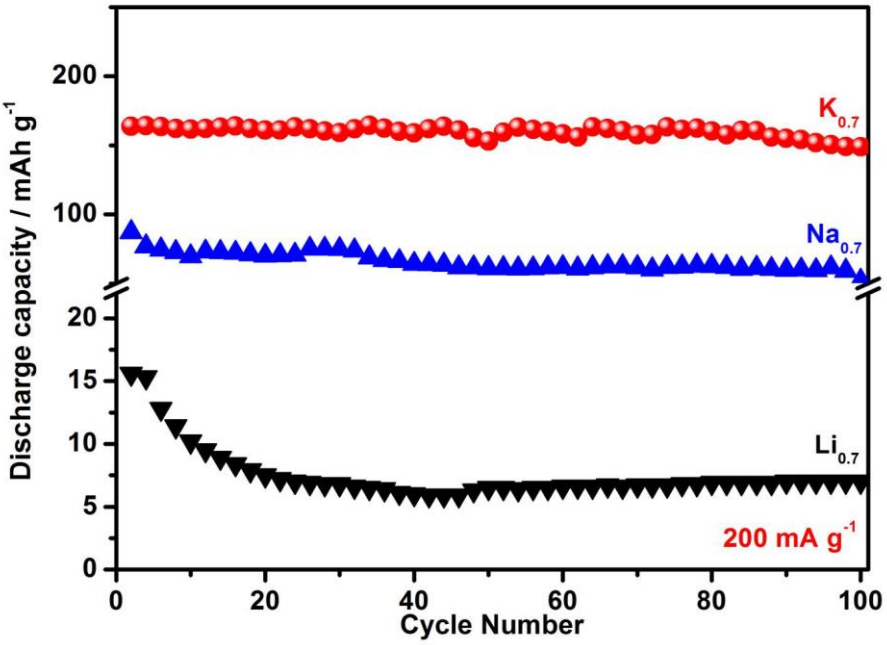

Figure S12. Cycling performance of the $K_{0.7}Fe_{0.5}Mn_{0.5}O_2$, $Na_{0.7}Fe_{0.5}Mn_{0.5}O_2$ and $Li_{0.7}Fe_{0.5}Mn_{0.5}O_2$ at 200 mA g^{-1}.

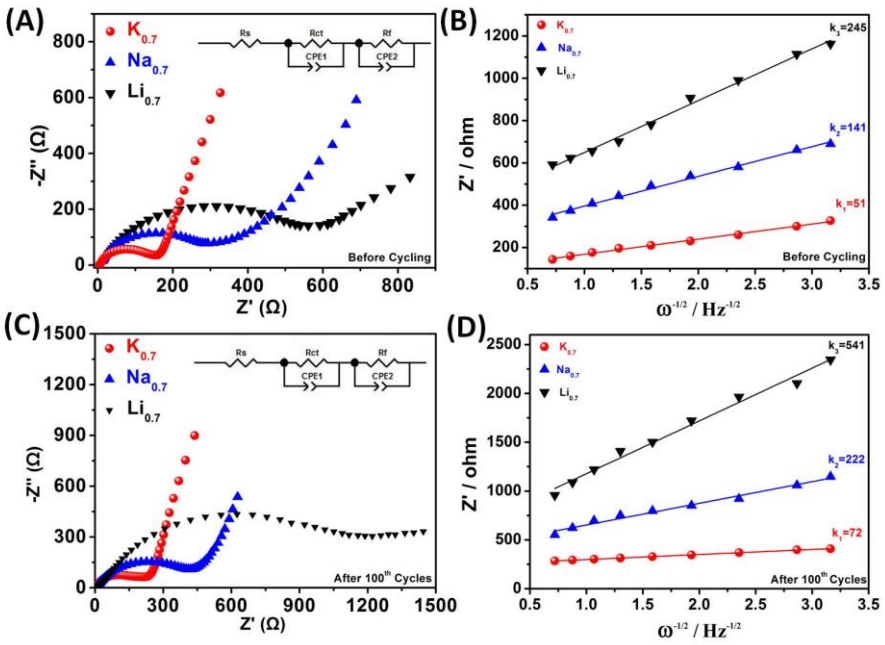

Figure S13. AC impedance plots (A) and kinetics calculations based on the frequency ($\omega^{-1/2}$) and Z′ values at low frequency region (B) of the three cathodes before cycle (from 0.1Hz to 100 kHz). AC impedance plots (C) and kinetics calculations based on the frequency ($\omega^{-1/2}$) and Z′ values at low frequency region (D) of the three cathodes after 100 cycles (from 0.1Hz to 100 kHz).

Calculation of the Sodium-ion Diffusion Kinetics

$$D_{Na} = R^2T^2/2A^2n^4F^4C^2\sigma^2 \qquad (1)$$

$$Z' = R_D+R_L+\sigma\omega^{-1/2} \qquad (2)$$

Here D_{Na} is the Na^+ diffusion coefficient, R is the gas constant, T is the absolute temperature, A is the surface area of cathode, n is the number of electrons per molecule during oxidization, F is the number of electrons per molecule during oxidization, C is the concentration of sodium ions, and σ is the Warburg factor that can be obtained by equation 2. The slope obtained by linear fitting of Z' and $\omega^{-1/2}$ (ω is frequency) is the σ value. The combination of equations 1 and 2 reveals that the square of the σ value has an inverse relationship with D_{Na}. According to equations 1 and 2, the slope of the linear fit of $\omega^{-1/2}$ and Z' is defined as the Warburg factor and its square values are inversely related to the Na^+-ion diffusion coefficient (D_{Na}).

Table S3. Comparison of the electrochemical performance of layered oxide cathode materials for sodium-ion batteries.

Active materials	Voltage ranges (V)	Current density (mA g^{-1})	Initial capacity (mAh g^{-1})	Cycle numbers	Capacity retention	Capacity fading per cycle
$K_{0.7}Fe_{0.5}Mn_{0.5}O_2$ (This Work)	1.5-4.0	100	181	100	93%	0.07%
		200	164	100	91%	0.09%
		500	134	100	98%	0.01%
		1000	117	1000	84%	0.02%
$Na[Ni_{1/3}Fe_{1/3}Mn_{1/3}]O_2$ [19]	1.5-4.0	75	130	150	76%	0.15%
$Na_{0.7}Fe_{0.5}Mn_{0.5}O_2$ [26]	1.5-4.2	26	195	80	86%	0.17%
$Na_{1/3}Mn_{0.8}Fe_{0.1}Ti_{0.1}O_2$ [33]	2.0-4.0	24.5	144	300	87%	0.04%
$Na_{0.7}Fe_{0.5}Mn_{0.5}O_2$ [34]	1.5-4.2	13	190	30	72%	0.93%
$NaNi_{0.25}Fe_{0.5}Mn_{0.25}O_2$ [38]	2.1-3.9	130	133	50	90%	0.19%
$Na[Ni_{0.75}Co_{0.02}Mn_{0.23}]O_2$ [40]	1.5-3.9	15	157	300	80%	0.07%

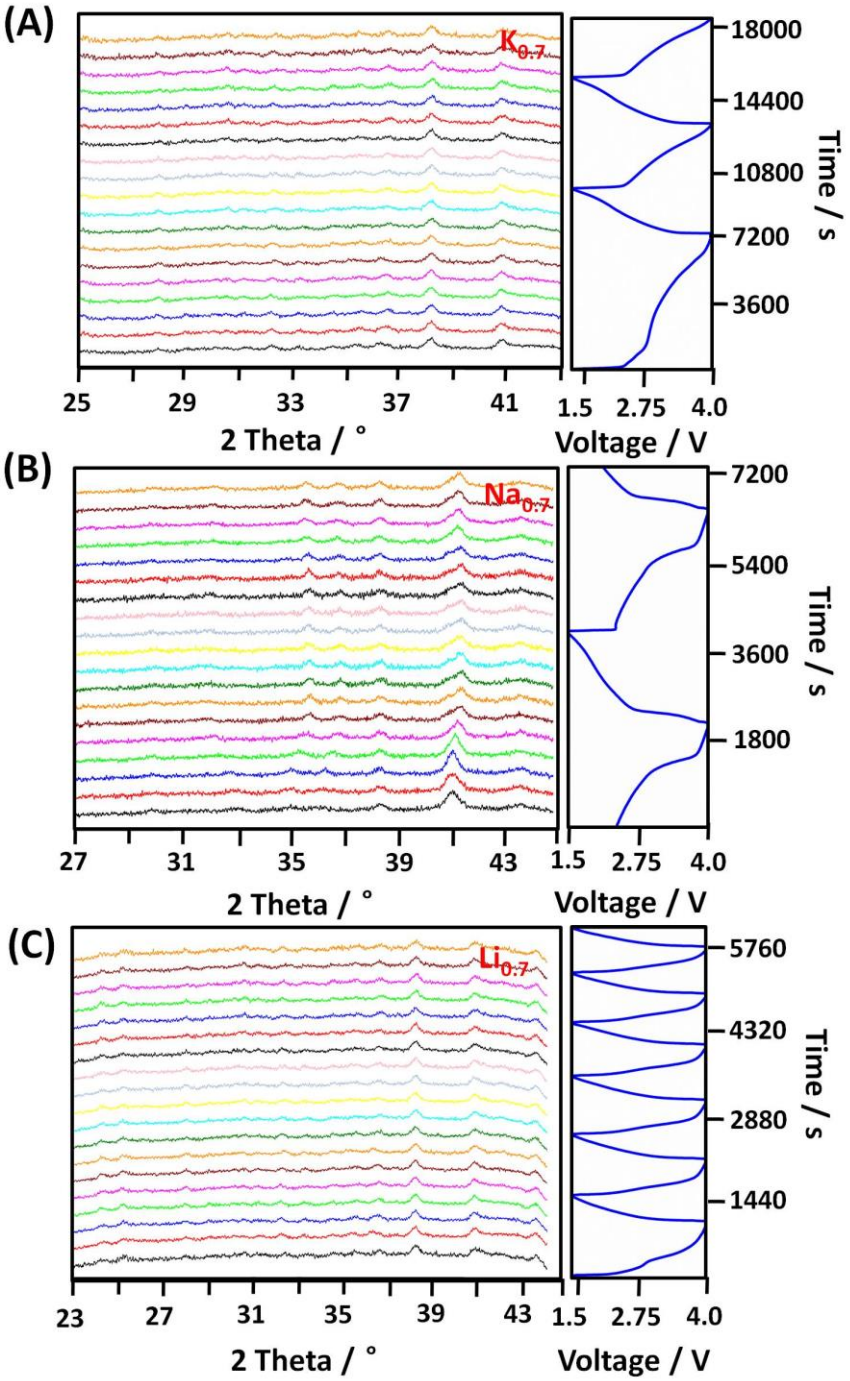

Figure S14. *In situ* XRD patterns results during galvanostatic charge and discharge. The image plot of the diffraction patterns of $K_{0.7}Fe_{0.5}Mn_{0.5}O_2$ (A) and $Na_{0.7}Fe_{0.5}Mn_{0.5}O_2$ (B) during charge-discharge at current density of 100 mA g^{-1}, respectively. (C) The image plot of the diffraction patterns of $Li_{0.7}Fe_{0.5}Mn_{0.5}O_2$ during charge-discharge at current density of 50 mA g^{-1}. The corresponding voltage curve is plotted to the right.